Evolution of Low-Noise Avalanche Photodetectors

Joe C. Campbell , Fellow, IEEE

(Invited Paper)

Abstract—This paper reviews materials and structural approaches that have been developed to reduce the excess noise in avalanche photodiodes and increase the gain-bandwidth product.

 ${\it Index} \quad {\it Terms} {\it --} {\bf Photodiode}, \quad {\bf photodetector}, \quad {\bf avalanche} \\ {\bf photodiode}.$

I. INTRODUCTION

OR APPLICATIONS that are not background limited, the most common sources of noise in an optical receiver are dark current, noise of the amplifier that follows the detector, or the quantum noise in the signal. Dark current issues are usually addressed by materials studies to reduce bulk sources, developing passivation techniques to suppress surface leakage, and cooling. Quantum noise in not an issue for most applications. If amplifier noise is the limiting mechanism, it is beneficial to use a detector with internal gain such as an avalanche photodiode (APD). It is that feature that has led to the utilization of APDs in a wide range of commercial, military, and research applications. Relative to many other types of photodetectors, APDs can provide higher signal to noise ratios and higher receiver sensitivities. From the mid 1970's to the present, optical communications [1], imaging [2], [3], and single photon detection [4], [5] have been the primary driving forces for research and development of APDs.

The origin of the gain in an APD is impact ionization in a multiplication region with high electric field intensity. Impact ionization is a stochastic process that results in excess noise, relative to shot noise, and limits the gain-bandwidth [6]–[8] This is due to the fact that, with few exceptions, both electrons and holes can impact ionize as shown in Fig. 1. An electron-hole pair is created by absorption of a photon in a low electric field region and, optimally, only the carrier that has the highest probability of impact ionizing, the electron in Fig. 1, is injected into a high field multiplication region. Avalanche multiplication is generally described in terms of the The electron and hole ionization coefficients, α and β , respectively, represent the mean rate of ionization per unit distance and are also equal to the inverse of the mean distance a carrier travels before ionizing.

Manuscript received May 31, 2021; accepted June 22, 2021. Date of publication June 28, 2021; date of current version July 20, 2021.

The author is with the Department of Electrical and Computer Engineering, University of Virginia, Charlottesville, VA 22904 USA (e-mail: jccuva@virginia.edu).

Color versions of one or more figures in this article are available at https://doi.org/10.1109/JSTQE.2021.3092963.

Digital Object Identifier 10.1109/JSTQE.2021.3092963

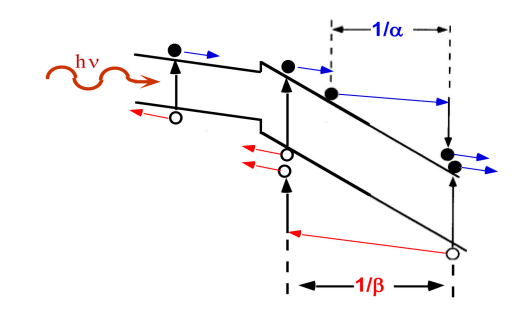


Fig. 1. Illustration of electron and hole impact ionization. $1/\alpha$ ($1/\beta$) is the average distance an electron (hole) travels before impact ionizing.

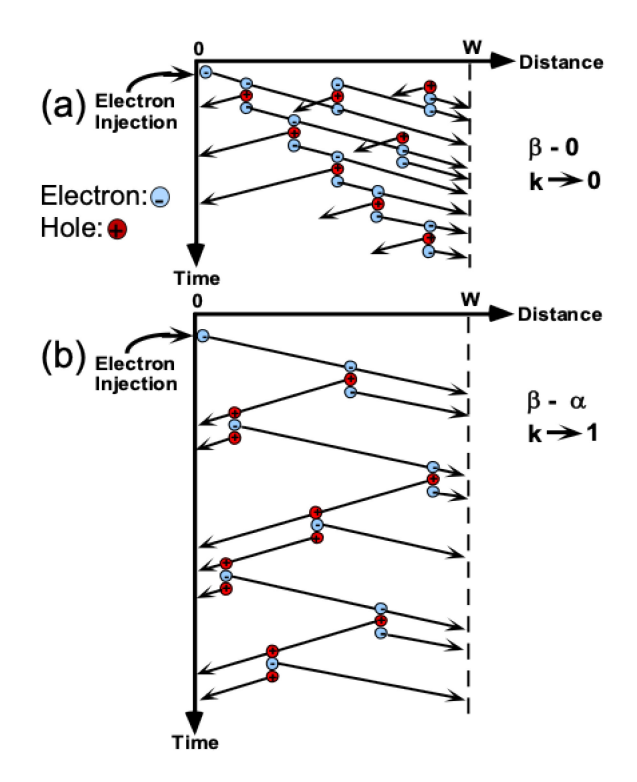


Fig. 2. Schematic diagram of avalanche process for (a) $\beta=0$ and (b) $\beta=\alpha$. Electrons designated by Θ and holes by \oplus .

The ionization coefficient ratio $k=\beta/\alpha$ is a key factor for the multiplication noise and bandwidth of an APD. This is illustrated in Fig. 2 for electron injection into a material with k=0 ($\beta=0$) and another with k=1 ($\beta=\alpha$). For k=1, since the process is somewhat chain-like, if an impact event does not occur, the variation in to total gain is much greater than for the k=0 case. This results in higher multiplication noise, which can be included

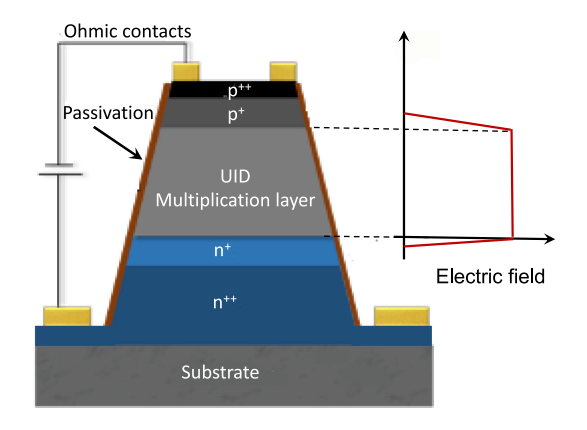


Fig. 3. Cross section and electric field for generic mesa-structure PIN APD.

as a multiplicative term, referred to as the excess noise factor, F(M), in the shot noise current, i_{shot} , which can be expressed as [6]:

$$i_{shot}^2 = 2q \left(I_{photo} + I_{dark} \right) M^2 F(M) \Delta f \tag{1}$$

where I_{photo} and I_{dark} are the photocurrent and dark current, respectively, M is the average value of the gain, and Δf is the bandwidth. In the local field model for pure electron injection, $F(M) = k \cdot M + (1-k) \cdot (2-1/M)$ [6]. Note that since the noise current scales as M^2 , small changes in k can significantly impact the noise.

Since the k = 1 case involves electrons and holes going back and forth across the multiplication region it takes longer to achieve the same number of impact events, and thus gain, than for k = 0, which requires only one transit for the electrons. The time required for the avalanche to build up increases with gain and gives rise to the gain-bandwidth product. The benefit of an APD is strongly dependent on whether it has sufficient gain-bandwidth, which is closely tied to the excess noise [8]. Consequently, increasing the gain-bandwidth product while reducing the excess noise has been a primary focus for APD research and development. The approaches to reduce the excess noise can be grouped into three categories. The earliest tactic was to select a semiconductor with favorable impact ionization coefficients. Later is was found that the excess noise factor could be significantly reduced by scaling the multiplication region to exploit the non-local aspect of impact ionization. The third approach can be broadly classified as impact ionization engineering using appropriately designed heterojunctions.

Much of the research on APDs of all types has utilized mesa structures, similar to the generic cross section shown in Fig. 3. Mesa photodiodes tend to have higher surface leakage, necessitating efforts to develop surface passivation techniques. Also, they are more susceptible to degradation from the environment, which affects reliability, than planar structures. However, the mesa structure is less complex and easier to fabricate than their planar counterparts. With only a couple of exceptions, the APDs described in this paper employ mesa structures.

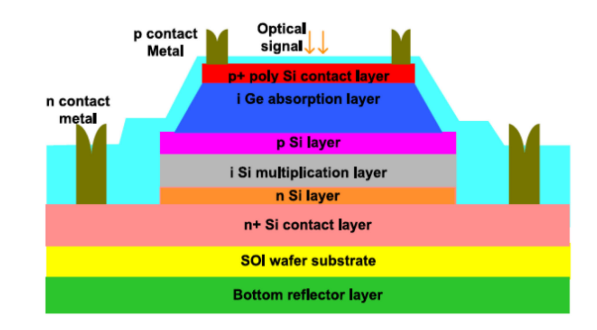


Fig. 4. Schematic cross section of Ge on Si SACM APD [18].

II. BULK MATERIALS

For bulk multiplication regions, the lowest noise has been achieved with materials such as Si, $Hg_{0.7}Cd_{0.3}Te$, InAs, $Al_xGa_{1-x}As_ySb_{1-y}$, and $Al_xIn_{1-x}As_ySb_{1-y}$ which have k << 1.

A. Silicon-Based APDs

K. M. Johnson reported the first signal-to-noise measurements on Si APDs [9]. He found significant improvement in the signalto-noise ratio relative to a Si p-i-n and that "the APD can be made nearly shot noise limited if the multiplication factor M is sufficiently large." Improved understanding of the limitations imposed on the signal-to-noise by gain fluctuations was achieved by McIntyre in his theory of multiplication noise [6]. The development of Si APDs has continued for a wide range of applications owing to their intrinsically low dark current density and excess noise characterized by a k value of 0.01 [10]–[15]. Research on Si APDs expanded rapidly for first-generation fiber optic receivers that operated at wavelengths of 800 nm to 900 nm. At 45 Mb/s bit rate, a Si APD receiver achieved 15 dB higher sensitivity than the same receiver with a p-i-n detector [16]. The evolution of fiber optic transmission wavelengths to 1300 nm and 1550 nm in order to take advantage of the optimum spectral windows for low dispersion and attenuation, however, motivated the transition to materials and device structures that operate at those wavelengths. The fact that Si has an indirect bandgap and, thus, relatively low absorption coefficient also constrains the bandwidth of Si detectors. However, owing to their low dark current, high detection efficiency, and low noise, Si APDs remain the detectors of choice for applications in the visible that do not require high speed.

Adapting Si APDs to operate at telecommunication wavelengths has been addressed by utilizing a Ge absorber in a separate absorption, charge, and multiplication (SACM) structure that utilizes Si as the multiplication region. This approach combines the strong absorption of Ge for wavelengths ≤ 1550 nm with the low-noise multiplication of Si. A Si charge layer ensures high electric field in the Si multiplication layer and low field in the Ge absorber, which is the primary source of dark current. Excess noise characterized by k as low as 0.08 and gain-bandwidth product of 340 GHz, which is two to three times higher than InP/InGaAs APDs, were achieved with a structure fabricated in a CMOS foundry [17]. Fig. 4 shows a schematic

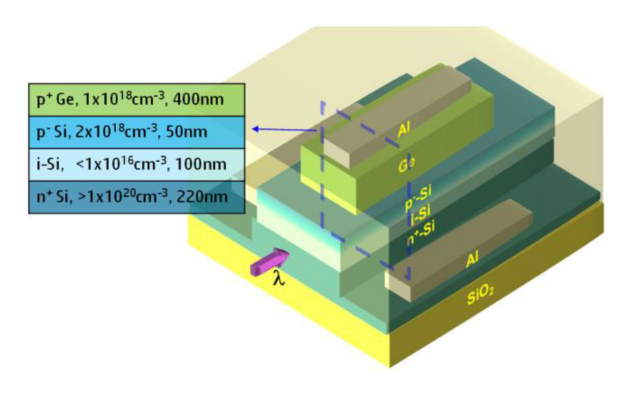


Fig. 5. Schematic of a waveguide Ge on Si SACM APD [19].

cross section of a Ge-on-Si SACM APD that utilizes resonant cavity enhanced responsivity[18] These APDs have achieved receiver sensitivities of -29.5 dBm ($\lambda = 1550$ nm) and -23.5 dBm ($\lambda = 1300$ nm) at 10 Gb/s and 25 Gb/s, respectively.

The rapid emergence of complex photonic integrated circuits has spurred development of waveguide detectors, with emphasis on structures that are compatible with silicon photonics. The Ge-on-Si APDs have proved to be excellent candidates for Si-based photonic circuits. Fig. 5 shows a waveguide Ge-on-Si SACM APD [19] This APD achieved breakdown voltage of -10 V, 25 GHz bandwidth, and a gain-bandwidth product of 276 GHz. Digital optical receivers that employ these detectors have achieved -16 dBm sensitivity at 50 Gb/s PAM4 with a bit error rate (BER) of 2.4×10^{-4} [20] In a coherent receiver, 64Gb/s PAM4 and 160Gb/s 16QAM detection has been reported [21] A Ge-on-Si APD integrated with a SiGe BiCMOS transimpedance amplifier has achieved sensitivity of -14.4 dBm and 10^{-12} BER at 50 Gb/s [22]

B. HgCdTe APDs

Hg_{1-x}Cd_xTe is unusual in that its impact ionization characteristics change extensively with composition. For example, for 0.6 < x < 0.7 the hole ionization coefficient is greater than that of the electron [23] However, for lower Cd fractions, this reverses to the extent that for x = 0.3, which corresponds to a cutoff wavelength of \sim 4.3 μ m, hole impact ionization vanishes, i.e., k = 0. The noise is quantified by an excess noise factor, F(M), in the range 1.1 and 1.4 [24], [25] The low noise appears to result from novel aspects of the bandstructure; the effective mass ratio ($m_h/m_e \sim 30$) is very large and unlike most III-V semiconductors, $Hg_{0.7}Cd_{0.3}Te$ has a very small Γ valley band gap (0.25 eV), and very high satellite L and X valleys (1.5 eV and 2.5 eV, respectively) [26] On the other hand, the small bandgap of Hg_{0.7}Cd_{0.3}Te necessitates cooling in order to reduce the dark current. These APDs are characterized by an exponentially increasing gain and the absence of avalanche breakdown. Fig. 6 shows the gain-voltage data on 53 of 54 connected diodes in an 8×8 array at 77 K. The mean optical gain at a uniform bias of 13.1 V was 1270 with a σ /mean uniformity of 4.5% [24] The high gains and low dark current density at low temperature have enabled linear mode single photon counting [27]

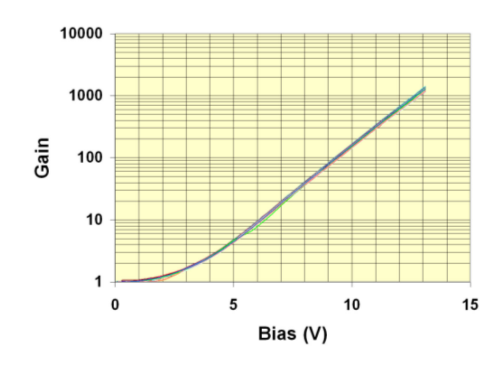


Fig. 6. Gain versus bias voltage for 53 connected $Hg_{0.7}Cd_{0.3}Te$ APDs in an 8×8 array at 77 K [24].

C. InAs APDs

In As is another material whose noise is characterized by k = 0with measured excess noise factor of 1.3 to 1.6 [28], [29] Similar to Hg_{0.7}Cd_{0.3}Te, the low bandgap of InAs tends to restrict operation to low temperatures. Gain normalized dark current density of 5×10^{-6} A/cm² at 77 K has been reported for mesa PIN structures [30] fabricated using a combination of phosphoric and sulphuric acid based etchants to reduce surface dark current [31] The combination of moderately weak field-dependence of the electron ionization coefficient and the onset of band-to-band tunneling at relatively low electric fields in InAs results thicker multiplication regions being required in order to achieve high multiplication gain. This, in turn necessitates low doping in order to realize complete depletion and a uniform electric field profile. It is difficult to achieve the requisite depletion width by reducing the background doping, however, p-type doping compensation of the n-type background has been used to obtain an 8 μ m-thick multiplication region, which yielded room temperature gain of 300 at -15 V bias [32], [33] As noted above, low k values also yield high gain bandwidth products [8] InAs APDs with gain-bandwidth product as high as 580 GHz have been reported [34]

The thick depletion widths exacerbate the difficulty of surface passivation for InAs APDs. To address this problem, planar structures have been developed using Beryllium implantation at a relatively low energy of 34 keV [35] Using a combination of post implant annealing at 500 °C for 15 min and a shallow surface etch produced planar APDs with room temperature dark current density of $0.52~\text{A/cm}^2$ at -0.2~V and external quantum efficiency of 51% at 1520~nm at -0.3~V. A maximum gain of 4 was achieved at -5V bias.

D. Quaternary Sb-Based APDs

Recently, two bulk quaternary materials, $Al_xGa_{1-x}As_ySb_{1-y}$ lattice-matched to InP and $Al_xIn_{1-x}As_ySb_{1-y}$ to GaSb have exhibited excess noise comparable to Si. The physical origin for the low noise has yet to be fully resolved. However, the strong dominance of electron impact ionization relative to holes, may be due to the Sb content, which can give rise to large phonon scattering rates and increased effective hole mass, resulting in a large reduction in β [36], [37]

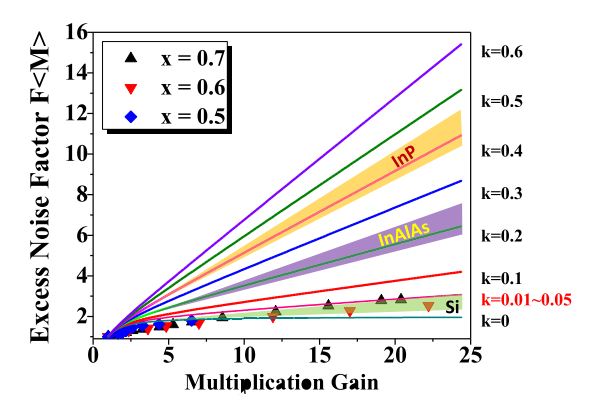


Fig. 7. Excess noise factor versus multiplication gain. The $\blacktriangle, \Delta,$ and \blacklozenge symbols represent the excess noise factor of $x=0.7,\,0.6$ and $0.5\,$ Al $_x$ In $_{1-x}$ As $_y$ Sb $_{1-y}$ APDs, respectively. Typical excess noise of InP, InAlAs and Si are shown by shaded region.

1) AlInAsSb APDs: Initial efforts to grow $Al_xIn_{1-x}As_ySb_{1-y}$ on GaSb, particularly for Al concentrations >30%, were impeded by a wide miscibility gap [38], [39] This difficulty was solved using molecular beam epitaxy (MBE) to grow $Al_xIn_{1-x}As_ySb_{1-y}$ (referred to below by the Al concentration as $Al_xInAsSb$) as a digital alloy, a short-period super-lattice structure composed of four binary alloys [40] The bandgap of $Al_xInAsSb$ on GaSb is direct for x=0 ($E_g=0.23$ eV) to x=0.8 ($E_g=1.3$ eV).

M. Ren et al., have reported Al_xInAsSb PIN-structure APDs with x = 0.7 to 0.3 [41] The gain normalized dark current was 5×10^{-5} A/cm² and 1.8×10^{-4} A/cm² for the x = 0.7 and x = 0.3 devices, respectively. Measurements of the dark current versus device diameter indicated that for the 70% devices surface leakage was the dominate dark current component whereas for the 30% device the dark current originated in the bulk, with a strong tunneling component. The 70% APDs exhibited gains as high as 100. Fig. 7 shows F(M) versus gain. The solid lines are plots of the excess noise for k-values from 0 to 0.6 using the local-field model [6] The k values for commercial Si APDs fall between 0.01 and 0.06. InP and InAlAs have been widely used in the multiplication layers of telecommunications APDs. InP typically exhibits k values between 0.4 and 0.5, while that for InAlAs is in the range 0.2 and 0.3, as denoted by the shaded regions in Fig. 7. The x = 0.5, 0.6, and 0.7 APDs have k values as low as 0.01. AlInAsSb PIN APDs grown as a random alloy by MBE on InP substrates have also exhibited low excess noise, k = 0.02, [42] calling into question the distinction between digital and random alloys and the origin of low noise in this material system.

Impact ionization is affected to a great extent by phonon scattering, which results in dependence of the gain and thus breakdown on temperature. This, in turn, necessitates temperature stabilizing techniques in optical receivers, an added cost and power penalty. Reducing this limitation can simplify receiver design. Fig. 8 shows the breakdown voltage temperature coefficient $\Delta V_{\rm bd}/\Delta T$ [43] versus multiplication layer thickness for $Al_xIn_{1-x}As_ySb_{1-y}$, InP, AlInAs, Si, and $Al_{1-x}Ga_xAs_ySb_{1-y}$ [44] When compared to devices with similar multiplication layer

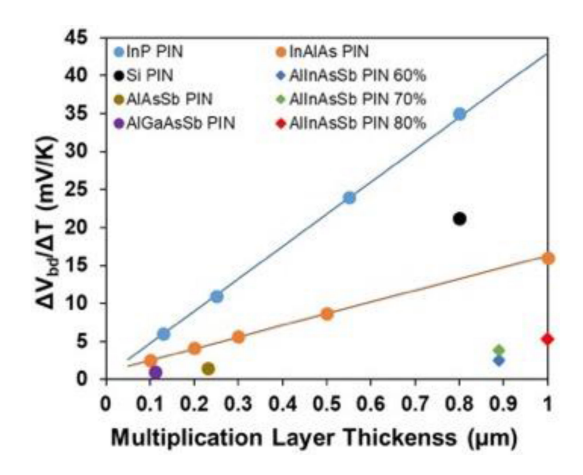


Fig. 8. Breakdown voltage temperature coefficient, $\Delta V_{\rm bd}/\Delta T$, for PIN APDs as a function of multiplication layer thickness.

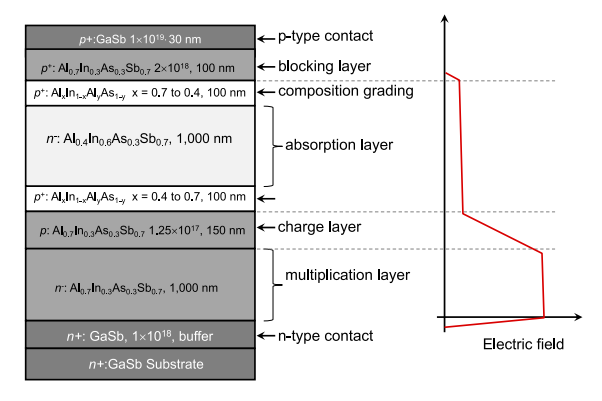


Fig. 9. Schematic cross section and electric field profile of AlInAsSb SACM APD.

thicknesses, $\Delta V_{\rm bd}/\Delta T$ of ${\sim}3 \text{mV/K}$ is less than a quarter that of AlInAs devices and almost an order of magnitude lower than $\Delta V_{\rm bd}/\Delta T$ for InP and Si devices.

The lower Al compositions ($x \le 0.5$) that operate at the optical communications wavelengths (1.3 to 1.6 μ m) exhibit excessive dark current due to tunneling at the high electric fields required for impact ionization. The solution is to employ an SACM structure with a lower Al content layer for absorption and higher Al layers for the multiplication region. Fig. 9 is a cross sectional schematic of an $Al_{0.7}In_{0.3}As_{0.3}Sb_{0.7}/Al_{0.4}In_{0.6}As_{0.3}Sb_{0.7}$ SACM APD. In order to reduce charge accumulation at the heterojunction interfaces, 100 nm-thick compositionally graded layers (x = 0.4 to 0.7) are positioned on each side of the absorption layer. The dark current, photocurrent, and gain versus bias voltage of a 50 μ m-diameter SACM APD are shown in Fig. 10. The dark current density at 95% breakdown was 6×10^{-3} A/cm², which is approximately $100 \times$ lower than that of Ge on Si APDs [17], [19] and comparable to that of AlInAs/InGaAs APDs [45] The maximum gain was 90 and the excess noise was the same as that of the homojunction APDs shown in Fig. 7.

In order to extend the operation of the AlInAsSb SACM APD to longer wavelength, the $Al_{0.4}InAsSb$ absorption layer was replaced with narrower bandgap $Al_{0.3}InAsSb$ (~ 0.58 eV)

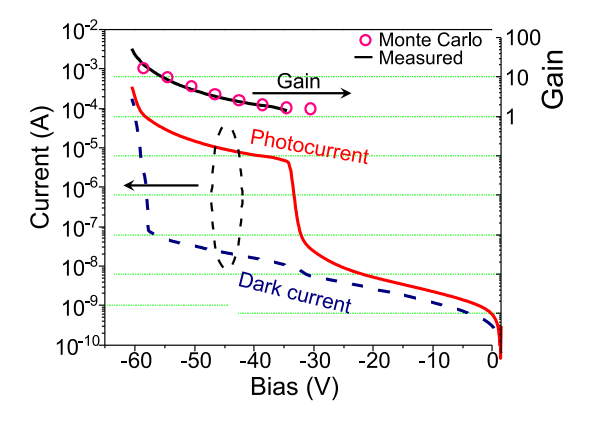


Fig. 10. Dark current, photocurrent, and measured and simulated (o) gain versus reverse bias of a 50- μ m-diameter $Al_xIn_{1-x}As_ySb_{1-y}$ SACM APD at 300 K.

[46] AlInAsSb exhibits the unique characteristic of a minimal valence band discontinuity within a wide range of bandgap energies (from 0.247 eV to 1.68 eV) [47] Since the change in the AlxInAsSb bandgap is primarily in the conduction band and impact ionization is heavily dominated by electrons, the design challenge lay primarily in the charge layer structure. This layer must deplete in such a way that the conduction band barrier sufficiently lowers to allow photo-generated carriers into the multiplication region without enabling band-to-band tunneling in the absorber. This was accomplished by optimizing the doping and thickness of the charge layer and continuous grading of the bandgap from the absorber to the multiplication region. The dark current density at 200 K was 3×10^{-4} A/cm² at M = 10, which is comparable to that of HgCdTe at 120K for the same gain. Under 2 μ m illumination, the gain was > 100 and the k-value was 0.01

2) AlGaAsSb APDs: The Al_xGa_{1-x}As_ySb_{1-y} material system has also exhibited very low multiplication noise. AlAs_{0.56}Sb_{0.44} PIN structure APDs with multiplication thickness of 1.5 μ m were grown by MBE on InP substrate [48] The dark current density was $\sim 10^{-3}$ A/cm² and the maximum gain was ~ 20 . The excess noise was measured using a mixed injection technique [49] A deduced β/α ratio as low as 0.005 was reported. It is interesting that while this is even lower than Si, these APDs exhibit abrupt breakdown unlike the linear-mode exponential gain observed in the k=0 HgCdTe [e.g., Fig. 6] and InAs APDs.

The high Al content in the AlAs $_{0.56}$ Sb $_{0.44}$ APDs renders them vulnerable to oxidation, which can produce high surface dark current [50] However, incorporating Ga into AlAs $_{0.56}$ Sb $_{0.44}$ can significantly reduce the dark current [51] Lee et al. have used that approach to fabricate low dark current Al $_{0.85}$ Ga $_{0.15}$ As $_{0.56}$ Sb $_{0.44}$ APDs with a 1 μ m-thick gain region [52] The epitaxial layers were grown lattice-matched to InP substrate by metal-organic chemical vapor deposition. Mesa structures were formed by chemical etching and the side walls were passivated with SU8. The bulk and surface components of the dark current were determined by fitting the total dark current to the expression:

$$I_{total} = M \cdot I_b + I_s \tag{2}$$

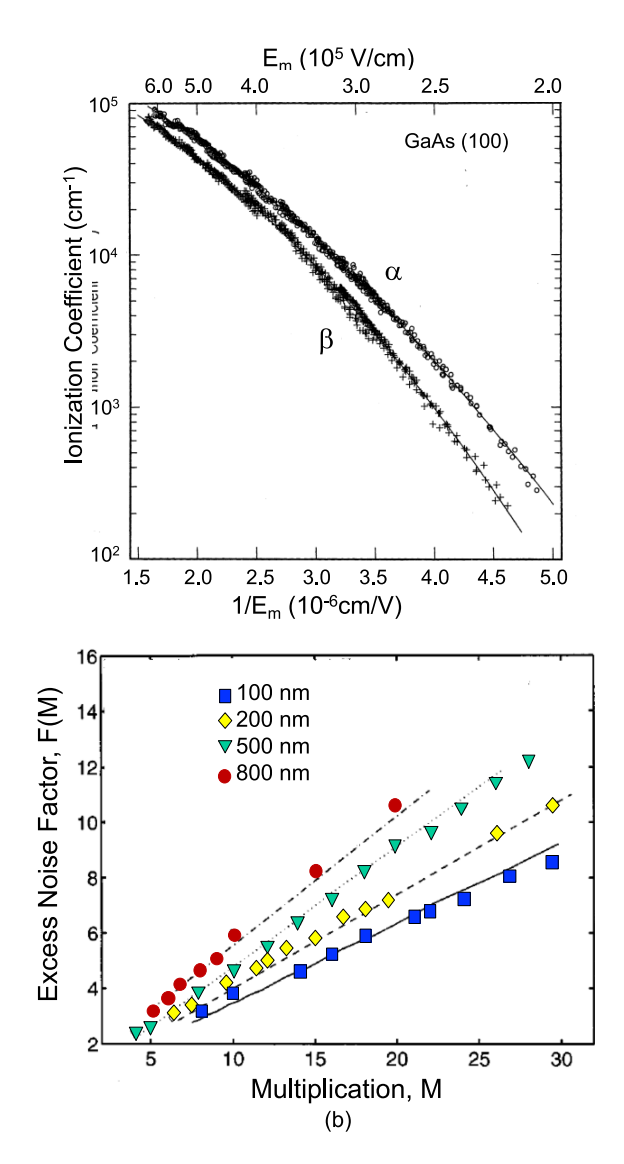


Fig. 11. (a) Measured ionization coefficients of bulk GaAs and [80] (b) measured excess noise factor, F(M), versus gain, M, for multiplication widths of 100 nm, 200 nm, 500 nm, and 800 nm [81].

where I_{total} is the measured dark current. I_b and I_s are the bulk and surface components of the dark current, respectively, and M is the gain. The bulk and surface dark current densities were 6.0 μ A/cm² and 0.23 μ A/cm, respectively. These values are about two orders of magnitude lower than those for previously reported 1550 nm thick AlAs_{0.56}Sb_{0.44} APDs [48] Excess noise measurements showed a low k of 0.01.

III. SUBMICRON SCALING OF THE MULTIPLICATION REGION

It has been shown for a wide range of materials including InP, [53]–[56] GaAs, [55]–[60] In_{1-x}Al_xAs, [55], [56], [61] Si, [62] Al_xGa_{1-x}As, [55], [56], [63]–[67] SiC, [68] GaP, [69] and GaInP [70] that reducing the thickness of the multiplication layer, usually to submicron dimensions, results in lower excess noise. [71]–[79] This is contrary to expectations based on the local-field model and points to its inadequacy when the non-local nature of impact ionization becomes significant. Fig. 11(a) shows the

ionization coefficients of GaAs as a function of the electric field [80] and the excess noise factor of GaAs for different multiplication layer widths in Fig. 11(b). [81] As shown in Fig. 11(a) at high electric field, the electron and hole ionization coefficients converge, which means that $k \sim 1$. This is due to the fact that at high electric field, phonon scattering becomes less significant, the carriers acquire near-ballistic velocities, and ionize quickly after achieving the ionization threshold energy, $E_{\rm th}$ [82] The energy required for ionization is determined by the constraints of conservation of energy and momentum and is roughly 1.5 times the bandgap energy. Typically, the electron and hole ionization energies are comparable, and it follows that their ionization coefficients are not too different at high fields.

As the thickness of the multiplication layer is reduced, in order to maintain the same gain, the electric field intensity must increase in order to reduce the distance between ionization events. However, since k approaches unity for high electric field, according to the local field model, decreased thickness should result in higher the excess noise factor, contrary to the trend shown in Fig. 11(b) where the opposite is observed. This is due to the fact that impact ionization is a non-local effect in that when carriers initially enter the multiplication region they are "cool" and require a certain distance to attain sufficient energy to ionize. This also applies to carriers immediately after ionization because their final states are typically near the band edge. Since little impact ionization occurs in the distance required to achieve threshold energy, this distance is referred to as the "dead space", $d_e(d_h)$ for electrons (holes). An approximation for the dead space is $d = E_{th}/qF$, where F is the electric field intensity. If the multiplication region is thick, the dead space can be neglected and the local field model provides an accurate description of the noise. However, for thin multiplication layers the non-local nature of impact ionization has a profound impact. This can be explained as follows: Since impact ionization is a stochastic process, it can be described in terms of a probability distribution function (pdf). For the local-field model, the pdf has the form $P(x) = \alpha^{-1} exp(-\alpha x)$ (Fig. 12(a)), where P(x) is the probability per unit length that a carrier ionizes a distance x from the injection point or the point where it was created by another impact ionization event. At the high fields encountered in thin multiplication regions, the pdf must be modified to account for the fact that $P(x) \sim 0$ for x < the dead space. This is illustrated qualitatively in Fig. 12(b). First, it is clear that the dead-space length decreases with increasing field because phonon scattering exerts less influence at high fields, which would tend to make the dead space less significant. However, the pdf also narrows significantly with increasing field. Since the width of the pdf decreases faster than the contraction in the dead space, the net result is that the ionization process becomes more deterministic, which reduces the variation in M and thus the excess noise.

Reducing the thickness of the multiplication region also plays a key role in determining the gain-bandwidth product, an essential parameter for communication and data transmission. At low gain, the speed of an APD will be determined by the RC time constant and the transit time for carriers across the depletion layer, similar to a p-i-n photodiode. However, in an APD as the carriers go back and forth across the multiplication layer, the

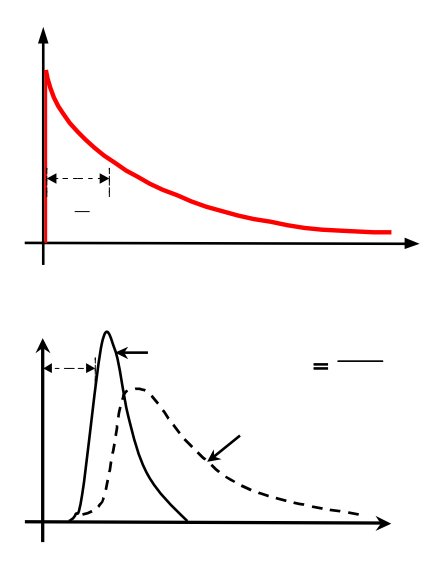


Fig. 12. Probability distribution functions for (a) the local field model and (b) inclusion of the dead space for high field (solid line) and low field (dashed line).

transit time transitions to an effective transit time that accounts for the time required for the avalanche process to build up or decay. At high gain, this gives rise to the gain-bandwidth product, which poses the fundamental limit to the bandwidth as the response time increases with multiplication region width and with the mean value of multiplication. The k value also affects the temporal response as illustrated in Fig. 2. As k increases, the gain becomes more of a serial process as multiple passes across the multiplication are required to achieve the gain value and this takes longer than the case for low k where almost all carriers traverse the multiplication region as a group within a single effective transit time.

The first commercial use of thin multiplication layers was InP/InGaAs SACM APDs for 2.5 Gb/s [83] and 10 Gb/s [84] telecommunication optical receivers. These APDs, which used \sim 250 nm-thick InP multiplication layer, achieved >10 dB higher receiver sensitivity than the same receivers with InGaAs p-i-n photodiodes. However, the relatively low gain-bandwidth product (<100 GHz), which is linked to the k value of InP (0.45), obviates operation at 25 Gb/s. While shrinking the multiplication region thickness is an effective approach to noise reduction, this is relative to the characteristic noise of the bulk (thick) material. Thus, lower noise can be achieved by beginning with lower k-value semiconductors. The bulk k for In_{0.52}Al_{0.48}As is \sim 0.3 and the fact that it is lattice matched to InP have made it the material of choice for telecommunication APDs [85]

A schematic cross section of an APD structure with a thin $In_{0.52}Al_{0.48}As$ multiplication region that has achieved record receiver sensitivity at 25 Gb/s and 50 Gb/s is shown in Fig. 13. [86], [87]

The thin (\sim 100 nm) In_{0.52}Al_{0.48}As multiplication region results in excess noise characterized by $k_{eff} \sim 0.15$ with a gain-bandwidth product of 240 GHz. The k value applies to the local-field model, which does not accurately describe the excess noise when non-local effects are in play. However, the constant k curves are typically superimposed on the excess

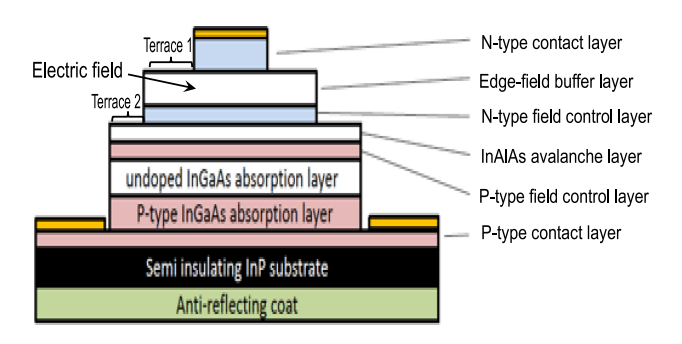


Fig. 13. Triple-mesa $\rm In_{0.52}Al_{0.48}$ As/ $\rm In_{0.53}Ga_{0.47}As$ SACM APD and electric field distribution at the operating bias.

noise plots because they provide a convenient indirect figure of merit for excess noise. In this case, the ratio of hole to electron ionization coefficients is greater than 0.15 but the excess noise is comparable to that of a bulk material with that k value.

In addition to the benefits of a thin multiplication layer, this structure has three additional aspects that contribute to its performance: two field control (charge) layers, a partially depleted p-type absorber, and a triple mesa structure. The triple mesa is designed to reduce the electric field at the device periphery in order to reduce surface leakage and prevent edge breakdown. By careful design of the edge-field buffer layer and the p-type and n-type field control layers, the high field can be confined to the center of the device. For the SACM APD, there is typically a single field control or "charge" layer to control the relative electric field intensities in the absorber and the multiplication layer. However, the use of an inverted p-down structure requires two field control layers. It is well known, that there is a tradeoff between responsivity and bandwidth in normal incidence photodetectors. Thicker absorption layers yield higher responsivity but concomitantly longer transit times, for which the hole velocity is the primary limiting factor. There are two absorber regions in Fig. 13. In the undepleted p-type region, the excess hole density decays rapidly with the dielectric relaxation time and electrons diffuse, at a velocity less than the electron saturation velocity, to the depletion region. In the depleted absorber, both carriers drift at their respective saturation velocities. In this case, the holes drift a shorter distance than they would if the whole absorber were depleted. By balancing the relative thicknesses of the depleted and undepleted absorption regions, the bandwidth and responsivity can be optimized [88]

Thin layers of $Al_xGa_{1-x}As_ySb_{1-y}$, which has exhibited low noise in bulk gain regions, are an alternative to InAlAs as the multiplication material. $Al_{0.85}Ga_{0.15}As_{0.56}Sb_{0.44}$ can be grown lattice matched to InP, which enables the use of semi-insulating substrates for high bandwidth and $In_{0.53}Ga_{0.47}As$ for the absorber. AlGaAsSb/InGaAs SACM APDs have been developed with multiplication and absorption layer thicknesses of 100 nm and 300 nm, respectively. These APDs exhibited k_{eff} of 0.05 to 0.08 [89] and gain bandwidth product \sim 420 GHz [90] Aside from InAs, which has demonstrated >500 GHz, this is the highest gain-bandwidth product reported for any APD. While dark current due to tunneling in the absorber can be addressed

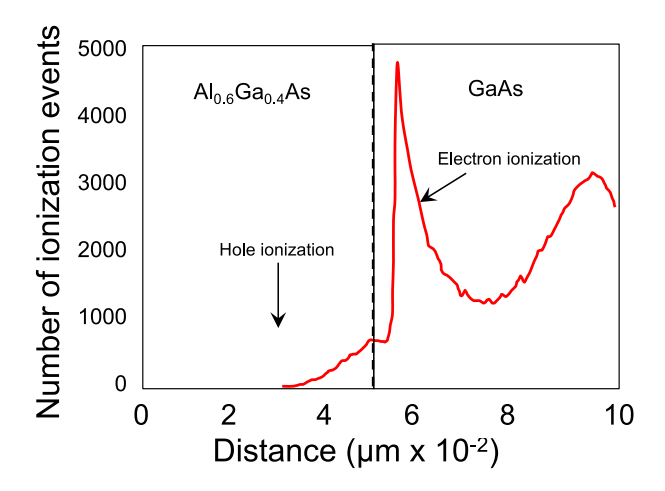


Fig. 14. Monte Carlo simulation of ionization rate for electron (solid) and hole (dotted) initiated impact ionization at an $Al_{0.6}Ga_{0.4}As/GaAs$ heterojunction, M=10. [98]

by precise control of the thickness of the charge layer and its carrier concentration, at the high electric field intensities required for avalanche gain, tunneling can become significant in the wide-bandgap multiplication layer. This was not observed in the AlGaAsSb/InGaAs SACM APDs.

IV. HETEROJUNCTION APDS

The noise of APDs with thin multiplication regions can be reduced even further by incorporating new materials and impact ionization engineering (I²E) with appropriately designed heterostructures [81], [91]–[97] The I²E structures that have achieved the lowest excess noise, to date, utilize multiplication regions in which electrons are injected from a wide bandgap semiconductor into adjacent low bandgap material. Initial work that demonstrated the efficacy of this approach utilized the GaAs/Al_xGa_{1-x}As material system. Excess noise equivalent to k < 0.1 has been demonstrated; in fact at low gain (M < \sim 10) the excess noise appears to correspond to k < 0, which, similar to the case for thin multiplication layers just highlights the flaws of the local field model for these structures [94], [94] For an electric field applied across a GaAs/AlGaAs heterojunction, as electrons are injected from the wide bandgap AlGaAs layer into the narrow bandgap region, the pdf exhibits a peak immediately after the heterojunction [98] This is illustrated in Fig. 14, which shows a Monte Carlo calculation of the number of electron and hole initiated ionization events for an Al_{0.6}Ga_{0.4}As/GaAs heterojunction. Electrons are injected at x = 0 and the heterojunction is located at $x = 0.055 \mu m$. The multiplication gain is \sim 10. The wide bandgap layer provides two benefits. Electrons gain energy in the wide bandgap layer but do not readily ionize owing to its high threshold energy. The hot electrons are then injected into the GaAs region, which has lower threshold energy, where they quickly ionize. The conduction band step provides additional energy to drive this process. The generated holes are immediately injected into the wide bandgap AlGaAs layer where hole ionization is more constrained. Both of these effects

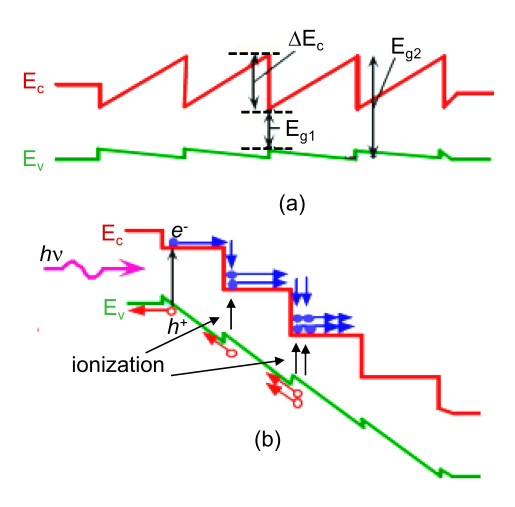


Fig. 15. (a) Band diagram of unbiased staircase APD and (b) illustration of localized impact ionization under reverse bias.

reduce excess noise by making the gain more single carrier induced and more deterministic. Hayat et al [99] have developed a modified dead-space multiplication theory (MDSMT) to describe injection of carriers with substantial kinetic energy into the multiplication region and have identified a mechanism, the "initial-energy effect" that reduces the excess noise, in the case of I²E structures, with a wide bandgap injector [100]

The I²E approach has been extended to the InGaAlAs material system. Duan et al. reported an SACM APD with a multiplication region consisting of unintentionally-doped layers of $In_{0.52}Al_{0.48}As$ (wide bandgap) and $In_{0.53}Ga_{0.17}Al_{0.3}As$ (layer narrow bandgap), both with thickness of 80 nm grown by MBE on InP substrate [96] The excess noise was characterized by $k_{eff} = 0.12$.

Another proposed approach for low-noise APDs is the cascade or tandem structure, which consists of a series of multiplication regions, all operated at relatively low gain in order to reduce the excess noise of each cell [101], [102] Combined with InAlAs/InAlGaAs I²E multiplication cells, this approach produced APDs with 84% external quantum efficiency at 1550 nm and excess noise characterized by k = 0.05. However, the thicker multiplication region of multiple gain cells also reduced the gain bandwidth product to 50 GHz [103] A five-element array of these APDs provided free-space position sensing with good uniformity and linearity down to an incident power of approximately -52 dBm and simultaneous data reception at 1.25 Gb/s, functions typically performed by two detectors [104] For 10^{-9} bit error rate, the sensitivity of the I²E arrays exceeded that of a commercially available single-element InAlAs/InGaAs APD [105] and p-i-n detectors [106] by 7 dB and 12 dB, respectively.

The structure that relies entirely on heterojunctions, specifically the conduction band discontinuity, for impact ionization is the staircase APD. In the early 1980's Capasso and co-workers proposed the staircase APD as a solid-state analog of the photomultiplier tube [107] The staircase APD structure consists of sequential bandgap graded regions (Fig 15(a)), which under reverse bias creates a series of steps as shown in Fig. 15(b).

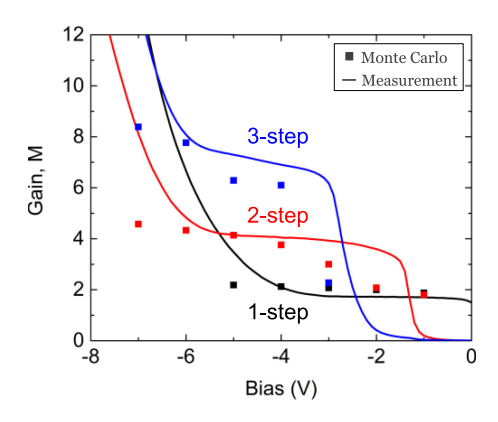


Fig. 16. Measured and Monte Carlo simulated gain for 1-, 2- and 3-step staircase APDs versus bias voltage at 300K.

Electrons that move from the wide to narrow bandgap regions acquire excess energy, which enables immediate, localized impact ionization. These discontinuities are somewhat analogous to dynodes in a photomultiplier, creating a more deterministic gain process with a resultant reduction in gain fluctuations, and thus lower excess noise. Ideally, the probability of impact ionization is unity at each step, generating a gain of 2ⁿ where n is the number of steps. If the probability for impact ionization is less than 1 and differs for each step, the gain is given by the expression:

$$M = \prod_{i=1}^{n} \left(1 + P_i \right)$$

where P_i is the impact ionization probability for the i_{th} step.

Initially $Al_xGa_{1-x}As/GaAs$ was used to fabricated the staircase band structures [108], [109] Unfortunately, the $Al_xGa_{1-x}As/GaAs$ conduction band discontinuity is not sufficient to impact ionize GaAs, particularly for high-energy electrons scattered to satellite valleys [110] The $Al_xIn_{1-x}As_ySb_{1-y}$ material system, on the other hand is well suited for the staircase APD structure. The direct bandgap is widely tunable from 0.24 (x = 0) to 1.25 eV (x = 0.8) [111] and the change in bandgap occurs almost entirely in the conduction band [112] As an example, for the $Al_{0.7}In_{0.3}As_{0.31}Sb_{0.69}/InAs_{0.9}1Sb_{0.09}$ heterojunction, the conduction band discontinuity is ~ 0.6 eV, which is 2.4x the bandgap energy of $InAs_{0.9}1Sb_{0.09}$. It follows that an electron will have sufficient energy to ionize as it crosses the step from the wide bandgap $Al_{0.7}In_{0.3}As_{0.31}Sb_{0.69}$ to the narrow bandgap $InAs_{0.9}1Sb_{0.09}$.

Initial work using AlInAsSb to create a single-step staircase APD demonstrated a gain of 1.8 ± 0.2 from -1 V to -4 V across a wide wavelength range [113] While the single step device showed the anticipated gain, it was not able to validate scaling with number of steps. Using 1-, 2-, and 3-step AlInAsSb staircase structures, March *et al.*, [114] have successfully demonstrated 2^n gain scaling. Fig. 16 shows the measured gain and Monte Carlo simulations for 1-, 2- and 3-step staircase APDs at 300K. The average measured gains for the 1-, 2-, and 3- step structures were 1.77, 3.97, and 7.14, and the average Monte Carlo simulated gains were 2.01, 3.81, and 6.71, respectively.

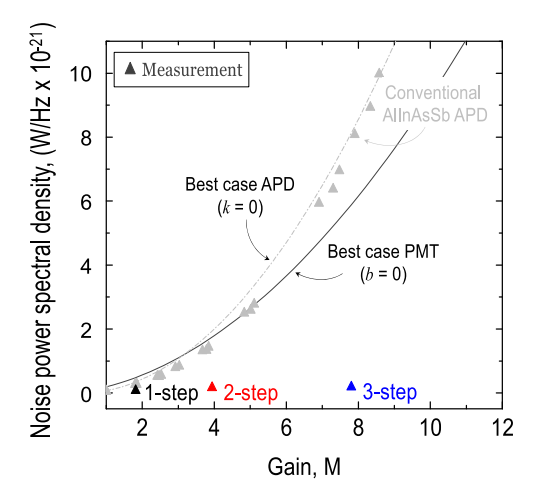


Fig. 17. Noise power spectral density versus gain measured directly with a calibrated noise figure meter for 1-, 2-, and 3-step staircase APDs. Also shown are the k=0 conventional APD (dashed curve), the measured $Al_{0.7}In_{0.3}As_{0.3}Sb_{0.7}$ homojunction digital alloy APD in Fig. 7 (p), and best case 3-dynode PMT (solid curve).

Fitting the gain versus step count yielded gain of 1.92ⁿ and 1.95ⁿ for measured data and Monte Carlo simulations, respectively, which provides confirmation of gain scaling with step count.

Similar to a photomultiplier tube (PMT) the gain mechanism of the staircase APD is spatially deterministic. However, for the PMT there can be significant uncertainty regarding the number of secondary electrons emitted at a dynode per incident electron. The staircase APD, on the other hand has a very narrow probability distribution at each step for impact ionization, which results in ultra-low noise. Fig. 17 shows the noise power spectral density measured with a calibrated noise figure meter versus gain for 1-, 2-, and 3-step staircase APDs at room temperature. Also shown are reference curves for the best case conventional APDs and best case 3-dynode PMT, along with measured values for the Al_{0.7}In_{0.3}As_{0.3}Sb_{0.7} homojunction digital alloy APD in Fig. 7.

V. CONCLUSION

While APDs have been successfully deployed for a wide range of applications, the quest to reduce the noise associated with the random nature of impact ionization has been unremitting. This is, of course, understandable since the gain-related excess noise can limit the receiver sensitivity of digital optical receivers, degrade signal to noise performance, and restrict the operating bandwidth. For many years the options were to try to find a material with low intrinsic noise, e.g., Si, or accept the restraints and performance penalties of other materials, e.g. InP for telecommunications. Approaches that take advantage of the non-local characteristic of impact ionization have led to significantly lower noise in a wide range of materials that now cover a broad spectrum. A technological "third wave" has opened the possibility of impact ionization engineering using new materials and creative design with heterojunctions to achieve even lower noise in more spectral regions with higher gain-bandwidth products.

ACKNOWLEDGMENT

This work was supported by the Army Research Office and DARPA (contract no. W911NF-17-1-0065) and DARPA (contract no. W909MY-12-D-0008) and by the National Science Foundation (Award No. ECCS-1933836).

REFERENCES

- J. C. Campbell, "Advances in photodetectors," in *Optical Fiber Telecommunications*, vol. 5, Part A: Components and Subsystems, 5th Edition,
 I. Kaminow, T. Li, and A. E. Wilner, editors, Cambridge, MA, USA: Academic Press, Feb. 22, 2008.
- [2] N. Bertone and W. R. Clark, "APD ARRAYS Avalanche photodiode arrays provide versatility in ultrasensitive applications," *Laser Focus World*, vol. 43, no. 9, pp. 69–73, Sep. 2007.
- [3] P. Mitra et al., "Adaptive focal plane array (AFPA) technologies for integrated infrared microsystems," vol. 6232, 2006, Paper 62320G-1-11.
- [4] A. Tosi, N. Calandri, M. Sanzaro, and F. Acerbi, "Low-noise, low-jitter, high detection efficiency InGaAs/InP single-photon avalanche diode," *IEEE J. Sel. Topics Quantum Electron.*, vol. 20, no. 6, Nov./Dec. 2014, Art. no. 3803406.
- [5] X. Jiang et al., "InP-based single-photon detectors and geiger-mode APD arrays for quantum communications applications," *IEEE J. Sel. Topics Quantum Electron.*, vol. 21, no. 3, May/Jun. 2015, Art. no. 3800112.
- [6] R.J. McIntyre, "Multiplication noise in uniform avalanche diodes," *IEEE Trans. Electron Dev.*, vol. 13, no. 1, pp. 164–168, Jan. 1966.
- [7] R.J. McIntyre, "Factors affecting the ultimate capabilities of high speed avalanche photodiodes and a review of the state-of-the-art," *Tech. Dig. Internat. Electron Dev. Mtg.*, vol. 19, pp. 213–216, 1973.
- [8] R. B. Emmons, "Avalanche-photodiode frequency response," J. Appl. Phys., vol. 38, pp. 3705–3714, 1967.
- [9] K. M. Johnson, "High-speed photodiode signal enhancement at avalanche breakdown voltage, *IEEE Trans. Electron Dev.*, vol. 12, no. 2, pp. 55–63, Feb. 1965.
- [10] C. A. Lee, R. A. Logan, R. L. Batdorf, J. J. Kleimack, and W. Weigmann, "Ionization rates of holes and electrons in silicon," *Phys. Rev.*, vol. 134, pp. A761–A773, 1964.
- [11] J. Conradi, "The distributions of gains in uniformly multiplying avalanche photodiodes: Experimental," *IEEE Trans. Electron Dev.*, vol. ED-19, no. 6, pp. 713–718, Jun. 1972.
- [12] W. N. Grant, "Electron and hole ionization rates in epitaxial silicon at high electric fields," *Solid-state Electron.*, vol. 16, pp. 1189–1203, 1973.
- [13] T. Kaneda, H. Matsumoto, and T. Yamaoka, "A model for reach-through avalanche photodiodes (RAPD's)," *J. Appl. Phys.*, vol. 47, no. 7, pp. 3135–3139, 1976.
- [14] P. P. Webb, R. J. McIntyre, and J. Conradi, "Properties of avalanche photodiodes," RCA Rev., vol. 35, no. 2, pp. 234–278, 1974.
- [15] V. M. Robbins, T. Wang, K. F. Brennan, K. Hess, and G. E. Stillman, "Electron and hole impact ionization coefficients in (100) and in (111) Si," J. Appl. Phys., vol. 58, pp. 4614–4617, 1985.
- [16] H. Melchior, A. R. Hartman, D. P. Schinke, and T.E Sidel, "Planar epitaxial silicon avalanche photodiode," *Bell System Tech. J.*, vol 57, no. 6, pp. 1791–1807, 1978.
- [17] Y. Kang et al., "Monolithic germaniumsilicon avalanche photodiodes with 340 GHz gain-bandwidth Product," Nature Photon., vol. 3, pp. 59–63, 2009.
- [18] M. Huang *et al.*, "Germanium on silicon avalanche photodiode," *IEEE Sel. Topics Quantum Elect.*, vol. 24, no. 2, pp. 1–11, Mar./Apr. 2018.
- [19] Z. Huang et al., "25 Gbps low-voltage waveguide SiGe avalanche photodiode," Optica, vol. 3, no. 8, pp 793–798, 2016.
- [20] B. Wang et al., "High-speed and energy efficient silicon photonic links," J. Lightw. Tech., vol. 38, no. 12, pp. 3156–3163, Jun. 2020.
- [21] J. Zhang, B. P.-P. Kuo, and S. Radic, "63Gb/s PAM4 and 160Gb/s 16 QAM modulation reception using a low-voltage Si-Ge waveguideintegrated APD," Opt. Exp., vol 28, no. 16, pp. 23266–23273, Aug. 2020.
- [22] S. A. Srinivasan et al., "56 Gb/s NRZ O-Band hybrid BiCMOS-silicon photonics receiver using Ge/si avalanche photodiode," J. Lightw. Tech., vol. 39, no. 5, pp. 1409–1415, Mar. 2021.
- [23] A. Singh, V. Śrivastav, and R. Pal, "HgCdTe avalanche photodiodes: A review," Opt. Laser Technol., vol. 43, no. 7, pp. 1358–1370, 2011.
- [24] J. Beck et al., "The HgCdTe electron avalanche photodiode," J. Electron. Mat., vol. 35, no. 6, pp. 1166–1173, Jun. 2006.

- [25] J. Rothman, "Physics and limitations of HgCdTe APDS: A review," J. Electron. Mat., vol. 47, no. 10, pp. 5657–5665, 2018.
- [26] F. Ma et al., "Monte carlo simulations of Hg_{0.7}Cd_{0.3}Te avalanche photodiodes and resonance phenomenon in the multiplication noise," Appl. Phys. Lett., vol. 83, pp. 785–787, 2003.
- [27] X. Sun et al., "HgCdTe avalanche photodiode array detectors with single photon sensitivity and integrated detector cooler assemblies for space lidar applications," Opt. Eng., vol. 58, no. 6, Jun. 2019, Art. no. 067103.
- [28] A. R. J. Marshall, C. H. Tan, M. J. Steer, and J. P. R. David, "Extremely low excess noise in InAs electron avalanche photodiodes," *IEEE Photon. Technol. Lett.*, vol. 21, no. 13, pp. 866–868, Jul. 2009.
- [29] S. J. Maddox, W. Sun, Z. Lu, H. P. Nair, J. C. Campbell, and S. R. Bank, "Enhanced low-noise gain from InAs avalanche photodiodes with reduced dark current and background doping," *Appl. Phys. Lett.*, vol. 101, no. 15, Oct. 2012, Art. no. 151124.
- [30] P. Jern Ker, A. R. J. Marshall, J. P. R. David, and C. H. Tan, "Low noise high responsivity InAs electron avalanche photodiodes for infrared sensing," *Physica Status Solidi (C) Curr. Topics Solid State Phys.*, vol. 9, no. 2, pp. 310–313, Feb. 2012.
- [31] A. R. J. Marshall, C. H. Tan, J. P. R. David, J. S. Ng, and M. Hopkinson, "Fabrication of InAs photodiodes with reduced surface leakage current," in *Proc. SPIE, Optial Mater. Defence Syst. Technol. IV*, 2007, vol. 6740, pp. 67400H-1-9.
- [32] S. Bank, S. J. Maddox, W. Sun, H. P. Nair, and J. C. Campbell, "Recent progress in high gain InAs avalanche photodiodes," in *Proc. SPIE*, vol. 9555, 2015, Art. no. 955509.
- [33] W. Sun, S. J. Maddox, S. R. Bank, and J. C. Campbell, "Record high gain from InAs avalanche photodiodes at room temperature," in *Proc. 72nd Device Res. Conf.*, Santa Barbara, CA, USA: 2014, pp. 47–8.
- [34] A. R. J. Marshall, P. J. Ker, A. Krysa, J. P. R. David, and C. H. Tan, "High speed InAs electron avalanche photodiodes overcome the conventional gain-bandwidth product limit," *Opt. Exp.*, vol. 19, no. 23, pp. 23341–23349, Nov. 2011.
- [35] L. W. Lim, C. H. Tan, Jo S. Ng, J. D. Petticrew, and A. B. Krysa, "Improved planar InAs avalanche photodiodes with reduced dark current and increased responsivity," *IEEE J. Lightw. Technol.*, vol. 37, no. 10, pp. 2375–2379, May 2019.
- [36] M. E. Woodson et al., "Low-Noise AlInAsSb avalanche photodiode," Appl. Phys. Lett., vol. 108, no. 8, Feb. 2016, Art. no. 081102.
- [37] X. Yi et al., Sci. Rep. vol. 8, pp. 9127–9133, 2018.
- [38] G. W. Turner, M. J. Manfra, H. K. Choi, and M. K. Connors, "MBE growth of high-power InAsSbInAlAsSb quantum-well diode lasers emitting at 3.5 μm," J. Cryst. Growth, vol. 175–176, no. Part 2, pp. 825–832, 1997.
- [39] A. N. Semenov et al., "Molecular beam epitaxy of AlInAsSb alloys near the miscibility gap boundary," J. Cryst. Growth, vol. 278, no. 2, pp. 2003–2008, 2005.
- [40] S. J. Maddox, S. D. March, and S. R. Bank, "Broadly Tunable AlInAsSb Digital Alloys Grown on GaSb," ACS Cryst. Growth Des., vol. 16, no. 7, pp. 3582–3586, 2016.
- [41] M. Ren et al., "Characteristics of Al_xIn_{1-x}As_ySb_{1-y} (x:0.3-0.7) avalanche photodiodes," *Lightw. Tech.*, vol. 35, no. 12, pp. 2380–2384, Jun. 2017
- [42] S. H. Kodati et al., "AlInAsSb avalanche photodiodes on InP substrates," Appl. Phys. Lett., vol. 118, no. 9, Mar. 2021, Art. no. 091101.
- [43] L. J. J. Tan etal., "Temperature Dependence of Avalanche Breakdown in InP and InAlAs," *IEEE J. Quantum Electron.*, vol. 46, no. 8, pp. 1153–1157, Aug. 2010.
- [44] A. Jones et al., "Al_xIn_{1-x}As_ySb_{1-y} photodiodes with low avalanche breakdown temperature dependence," Opt. Exp., vol. 25, no. 20, pp. 24340–24345, Oct. 2017.
- [45] M. Nada, Y. Muramoto, H. Yokoyama, T. Toshimatsu, and H. Matsuzaki, "High-speed avalanche photodiodes for 100-Gb/s systems and beyond," in *Proc. Eur. Conf. Opt. Commun.*, 2014, p. 3.
- [46] A. H. Jones, S. D. March, S. R. Bank, and J. C. Campbell, "AlI-nAsSb/GaSb separate absorption, charge, and multiplication avalanche photodiodes for 2-μm applications," *Nature Photon.*, vol. 14, no. 9, pp. 559–563, Sep. 2020.
- [47] J. Zheng et al., "Characterization of band offsets in AlxIn1-xAsySb1-y alloys with varying Al composition," Appl. Phys. Lett., vol. 115, no. 12, Sept. 2019, Art. no. 122105.
- [48] X. Yi et al., "Extremely low excess noise and high sensitivity AlAs_{0.56}Sb_{0.44} avalanche photodiodes," Nat. Photon., vol. 13, pp. 683–686, Oct. 2019.
- [49] G. E. Stillman and C. M. Wolfe, "Avalanche photodiodes," in *Semiconductors and Semimetals*, R. K. Willardson and A. C. Beer, Eds. New York: Academic, vol. 12, pp. 332–334, 1977.

- [50] X. Zhou, S. Zhang, J. P. R. Davie, J. S. Ng, and C.-H. Tan, "Avalanche breakdown characteristics of Al_{1-x}Ga_xAs_{0.56}Sb_{0.44} quaternary alloys," *IEEE Photon. Tech. Lett*, vol. 28, no. 22, pp. 2495–2498, Aug. 2016.
- [51] S. K. Mathis et al., "Lateral oxidation kinetics of AlAsSb and related alloys lattice matched to InP," J. Appl. Phys., vol. 89, pp. 2458–2464, 2001
- [52] S. Lee et al., "Low noise Al_{0.85}Ga_{0.15}As_{0.56}Sb_{0.44} avalanche photodiodes on InP substrates," Appl. Phys. Lett., vol. 118, no. 8, Feb. 2021.
- [53] K. F. Li et al., "Low avalanche noise characteristics in thin InP p + -i-n + diodes with electron-initiated multiplication," *IEEE Photon. Technol. Lett.*, vol. 11, pp. 364–366, 1999.
- [54] J. C. Campbell, S. Chandrasekhar, W. T. Tsang, G. J. Qua, and B. C. Johnson, "Multiplication noise of wide-bandwidth InP/InGaAsP/InGaAs avalanche photodiodes," *J. Lightw. Technol* vol. 7, no. 3, pp. 473–477, Mar. 1989.
- [55] P. Yuan et al., "Impact ionization characteristics of III–V semiconductors for a wide range of multiplication region thicknesses," *IEEE J. Quant. Electron.*, vol. 36, no. 2, pp. 198–204, Feb. 2000.
- [56] M. A. Saleh et al., "Impact-ionization and noise characteristics of thin III–V avalanche photodiodes," *IEEE Trans. Electron Dev.*, vol. 48, no. 12, pp. 2722–2731, Dec. 2001.
- [57] K. F. Li et al., "Avalanche noise characteristics of thin GaAs structures with distributed carrier generation," *IEEE Trans. Electron Dev.*, vol. 47, no. 5, pp. 910–914, May 2000.
- [58] K. F. Li et al., "Avalanche multiplication noise characteristics in thin GaAs p⁺-i-n⁺ diodes," *IEEE Trans. Electron Dev.*, vol. 45, no. 10, pp. 2102–7, Oct. 1998.
- [59] C. Hu, K. A. Anselm, B. G. Streetman, and J. C. Campbell, "Noise characteristics of thin multiplication region GaAs avalanche photodiodes," *Appl. Phys. Lett.*, vol. 69, no. 24, pp. 3734–3736, 1996.
- [60] S. A. Plimmer et al., "Investigation of impact ionization in thin GaAs diodes," *IEEE Trans. Electron Dev.*, vol. 43, no. 7, pp. 1066–1072, Jul. 1996.
- [61] C. Lenox et al., "Thin multiplication region InAlAs homojunction avalanche photodiodes," Appl. Phys. Lett., vol. 73, pp. 783–784, 1998.
- [62] C. H. Tan et al., "Avalanche noise measurements in thin Si p⁺-i-n⁺ diodes," Appl. Phys. Lett., vol. 76, no. 26, pp. 3926–3928, 2000.
- [63] X. G. Zheng et al., "Multiplication Noise of Al_xGa_{1-x}As Avalanche photodiodes with high Al concentration and thin multiplication region," Appl. Phys. Lett., vol. 78, pp. 3833–3835, 2001.
- [64] S. A. Plimmer *et al.*, "Impact ionization in thin $Al_xGa_{1-x}As$ (x = 015 –0.30) p-i-n diodes," *J. Appl. Phys.*, vol. 82, no. 3, pp. 1231–1235, 1997
- [65] B. K. Ng et al., "Avalanche multiplication and breakdown in Al_xGa_{1-x}As (x < 0.9)," IEEE Trans. Electron Dev., vol. 49, no. 12, pp. 2349–2351, 2002.
- [66] B. K. Ng et al., "Excess noise characteristics of Al_{0.8}Ga_{0.2}As avalanche photodiodes," *IEEE Trans. Elect. Dev.*, vol. 48, no. 10, pp. 2198–2204, 2001.
- [67] C. H. Tan et al., "Low multiplication noise thin Al_{0.6}Ga_{0.4}As avalanche photodiodes," *IEEE Trans. Electron Dev.*, vol. 48, no. 7, pp. 1310–1317, Jul. 2001.
- [68] B. K. Ng et al., "Nonlocal effects in thin 4H-SiC UV avalanche photodiodes," *IEEE Trans. Electron Dev.*, vol. 50, no. 8, pp. 1724–1732, Aug. 2003.
- [69] A. L. Beck et al., "Quasi-direct UV/blue GaP avalanche photodiodes," IEEE J. Quantum Electron., vol. 40, no. 12, pp. 1695–1699, Dec. 2004.
- [70] C. H. Tan, R. Ghin, J. P. R. David, G. J. Rees, and M. Hopkinson, "The effect of dead space on gain and excess noise in In_{0.48}Ga_{0.52}P p⁺in⁺ diodes," *Semicond. Sci. Tech.*, vol. 18, no. 8, pp. 803–806, 2003.
- [71] M. M. Hayat, B. E. A. Saleh, and M. C. Teich, "Effect of dead space on gain and noise of double-carrier multiplication avalanche photodiodes," *IEEE Trans. Electron. Dev.*, vol. 39, no. 3, pp. 546–552, Mar. 1992.
- [72] R. J. McIntyre, "A new look at impact ionization part 1: a theory of gain, noise, breakdown probability and frequency response," *IEEE Trans. Electron Dev.*, vol. 48, no. 8, pp. 1623–1631, Aug. 1999.
- [73] P. Yuan et al., "A new look at impact ionization part ii: Gain and noise in short avalanche photodiodes," *IEEE Trans. Electron Dev.*, vol. 46, no. 8, pp. 1632–1639 Aug. 1999.
- [74] X. Li, X. Zheng, S. Wang, F. Ma, and J. C. Campbell, "Calculation of gain and noise with dead space for GaAs and Al_xGa_{1-x}As avalanche photodiodes," *IEEE Trans. Electron Dev.*, vol. 49, no. 7, pp. 1112–1117, Jul. 2002.

- [75] B. Jacob, P. N. Robson, J. P. R. David, and G. J. Rees, "Fokker-Planck model for nonlocal impact ionization in semiconductors," *J. Appl. Phys.*, vol. 90, no. 3, pp. 1314–1317, 2001.
- [76] A. Spinelli and A. L. Lacaita, "Mean gain of avalanche photodiodes in a dead space model," *IEEE Trans. Electron Dev.*, vol. 43, no. 1, pp. 23–30, Jan. 1996.
- [77] D. S. Ong et al., "A Monte Carlo investigation of multiplication noise in thin p⁺in⁺ avalanche photodiodes," *IEEE Trans. Electron Dev.*, vol. 45, no. 8, 1998.
- [78] S. A. Plimmer, J. P. R. David, D. S. Ong, and K. F. Li, "A simple model including the effects of dead space," *IEEE Trans. Electron. Dev.*, vol. 46, no. 4, pp. 769–775, Apr. 1999.
- [79] G. J. Rees and J. P. R. David, "Nonlocal impact ionization and avalanche multiplication," *J. Phys. D: Appl. Phys.*, vol. 43, no. 2417, 5 May 2010, Art. no. 243001.
- [80] G. E. Bulman, V. M. Robbins and G. E. Stillman, "The determination of impact ionization coefficients in (100) gallium arsenide using avalanche noise and photocurrent multiplication measurements," *IEEE Trans. Electron Dev.*, vol. 32, no. 11, pp. 2454–2466, Nov. 1985.
- [81] M. M. Hayat *et al.*, "Boundary effects on multiplication noise in thin heterostructure avalanche photodiodes: theory and experiment," *IEEE Trans. Electron Dev.*, vol. 49, no. 2, pp. 2114–2123, Dec. 2002.
 [82] C.L. Anderson and C.R. Crowell, "Threshold energies for electron-hole
- [82] C.L. Anderson and C.R. Crowell, "Threshold energies for electron-hole pair production by impact ionization in semiconductors," *Phys. Rev.*, vol. B5, pp. 2267–2272, 1972.
- [83] M. A. Itzler, C. S. Wang, S. McCoy, N. Codd, and N. Komaba, "Planar bulk InP avalanche photodiode design for 2.5 and 10 Gb/s applications," in Proc. ECOC '98 - 24th Eur. Conf. Opt. Commun., vol. 1, pp. 59–60, Madrid, Spain Sep. 1998.
- [84] M. A. Itzler, K. K. Loi, S. McCoy, N. Codd, and N. Komba, "Manufacturable planar bulk-InP avalanche photodiodes for 10 Gb/s applications," in *Proc. IEEE LEOS Annu. Meeting Conf.*, 1999, vol. 2, pp. 748–749.
- [85] I. Watanabe, T. Torikai, K. Makita, K. Fukushima, and T. Uji, "Impact ionization rates in (100) Al0.48In0.52As," *IEEE Electron Dev. Lett.*, vol. 11, no. 10, pp. 437–439, 1990.
- [86] M. Nada, Y. Muramoto, H. Yokoyama, T. Ishibashi, and S. Kodama, "InAlAs APD with high multiplied responsivity-bandwidth product (MR-bandwidth product) of 168 A/W GHz for 25 Gbit/s high-speed operations," *Electron. Lett.*, vol. 48, no. 7, pp. 397–399, Mar. 2012.
- [87] M. Nada, Y. Yamada, and H. Matsuzaki, "Responsivity-bandwidth limit of avalanche photodiodes: toward future ethernet systems," *IEEE J. Sel. Topics Quantum Electron.*, vol. 24, no. 2, Mar./Apr. 2018, Art. no. 3800811.
- [88] Y. Muramoto and T. Ishibashi, "InP/InGaAs pin photodiode structure maximising bandwidth and efficiency," *Electron. Lett.*, vol. 39, pp. 1749–1750, 2003.
- [89] L. L. G. Pinel et al., "Effects of carrier injection profile on low noise thin Al_{1-x}Ga_xAs_{0.56}Sb_{0.44} avalanche phtodiodes, Opt. Exp., vol. 26, no. 3, pp. 24242–24247, Feb. 2018.
- [90] S. Xie et al., "InGaAs/AlGaAsSb avalanche photodiode with high gain-bandwidth product," Opt. Exp., vol. 24, no. 21, pp. 24242–24247, 2016.
- [91] P. Yuan et al., "Avalanche photodiodes with an impact-ionizationengineered multiplication region," *IEEE Photon. Tech. Lett.*, vol. 12, no. 10, pp. 1370–1372, Oct. 2000.
- [92] O.-H. Kwon et al., "Optimal excess noise reduction in thin heterojunction Al_{0.6}Ga_{0.4}As-GaAs avalanche photodiodes," *IEEE J. Quantum Electron.*, vol. 39, no. 10, pp. 1287–1296, Oct. 2003.
- [93] C. Groves, C. K. Chia, R. C. Tozer, J. P. R. David,and G. J. Rees, "Avalanche noise characteristics of single Al_xGa_{1-x}As(0.3 < x < 0.6)— GaAs heterojunction APDs," *IEEE J. Quantum Electron.*, vol. 41, no. 1, pp. 70–75, 2005.
- [94] S. Wang et al., "Ultra-low noise avalanche photodiodes with a 'centered-well' multiplication region," *IEEE J. Quantum Electron.*, vol. 39, no. 2, pp. 375–378, Feb. 2003.
- [95] S. Wang et al., "Low-noise impact-ionization-engineered avalanche photodiodes grown on InP substrates," *IEEE Photon. Tech. Lett.*, vol. 14, no. 12, pp. 1722–1724, Dec. 2002.
- [96] N. Duan et al., "High-speed and low-noise SACM avalanche photodiodes with an impact-ionization engineered multiplication region," *IEEE Photon. Tech. Lett.*, vol. 17, no. 8, pp. 1719–1721, Aug. 2005.
- [97] W. R. Clark, K. Vaccaro, and W. D. Waters, "InAlAs-InGaAs based avalanche photodiodes for next generation eye-safe optical receivers," in *Proc. SPIE*, vol. 6796, 2007, Art. no. 67962H.

- [98] C. Groves, J. P. R. David, G. J. Rees, and D. S. Ong, "Modeling of avalanche multiplication and noise in heterojunction avalanche photodiodes," *J. Appl. Phys.*, vol. 95, no. 11, pp. 6245–6251, Jun. 2004.
- [99] M. M. Hayat et al., "Boundary effects on multiplication noise in thin heterostructure avalanche photodiodes," *IEEE Trans. Electron Dev.*, vol. 49, no. 12, pp. 2114–2123, Dec. 2002.
- [100] O.-H. Kwon et al., "Optimal excess noise reduction in thin heterojunction Al_{0.6}Ga_{0.4}As-GaAs avalanche photodiodes," *IEEE J. Quantum Electron.*, vol. 39, no. 10, pp. 1287–1296, Oct. 2003.
- [101] J. P. Gordon, R. E. Nahory, M. A. Pollack, and J. M. Worlock, "Low-noise multistage avalanche photodetector," *IEEE Electron. Lett.*, vol. EL-15, no. 17, pp. 518–519, 1979.
- [102] S. Rakshit and N. B. Charkraborti, "Multiplication noise in multiheterostructure avalanche photodiodes," *Solid State Electron.*, vol. 26, no. 10, pp. 999–1003, 1983.
- [103] Wenlu Sun, X. Zheng, Z. Lu, and J. C. Campbell, "Monte Carlo simulation of InAlAs/InAlGaAs tandem avalanche photodiodes," *J. Quantum Electron.*, vol. 48, no. 4, pp. 528–532, 2012.
- [104] M. S. Ferraro et al., "Position sensing and high bandwidth data communication using impact ionization engineered APD arrays," *IEEE Photon. Tech. Lett.*, vol. 31, no. 1, pp. 58–61, Jan. 2019.
- [105] InGaAs Avalanche Photodiode 1.25 Gbps BM APD-TIA, PDAF0055TOL-T20 Datasheet, GoPhoton, Inc., Somerset, NJ, USA, Oct. 2014.
- [106] 1.25 Gbps/2.50, Gbps Hybrids: InGaAs Photodetectors/Transimpedance Amplifiers, Version 3, Rev. 052915, OSI Parts Catalog, OSI Optoelectronics, Inc., Hawthorne, CA, USA, 2007, pp. 94–95.
- [107] F. Capasso, W. T. Tsang, and G. F. Williams, "Staircase solid-state photomultipliers and avalanche photodiodes with enhanced ionization rates ratio," *IEEE Trans. Electron Dev.*, vol. ED-30, no. 4, pp. 381–390, Apr. 1983.
- [108] G. F. Williams, F. Capasso, and W. T. Tsang, "The graded bandgap multilayer avalanche photodiode: A new low-noise detector," *IEEE Electron Dev. Lett.*, vol. EDL-3, no. 3, pp. 71–73, Mar. 1982.
- [109] G. Ripamonti et al., "Realization of a staircase photodiode. Towards a solid-state photomultiplier," Nucl. Inst. Methods Phys. Res., vol. 288, no. 1, pp. 99–103, Mar. 1990
- [110] I. K. Czajkowski, J. Allam, and A. R. Adams, "Role of satellite valleys in ionisation rate enhancement in multiple quantum well avalanche photodiodes," *Electron. Lett.*, vol. 26, no. 16, p 1311–1313, Aug. 1990
- [111] S. J. Maddox, S. D. March, and S. R. Bank, "Broadly tunable AlInAsSb digital alloys grown on GaSb," *Cryst. Growth Des.*, vol. 16, no. 7, pp. 3582–3586, Jul. 2016
- [112] J. Zheng et al., "Characterization of band offsets in Al_xIn_{1-x}As_ySb_{1-y} alloys with varying Al composition," Appl. Phys. Lett., vol. 115, no. 12, Sep. 2019, Art. no. 122105.
- [113] M. Ren et al., "AlInAsSb/GaSb staircase avalanche photodiode," Appl. Phys. Lett., vol. 108, no. 8, Art. no. 081101, Feb. 2016.
- [114] S. D. March, A. H. Jones, J. C. Campbell, and S. R. Bank, "Multistep staircase avalanche photodiodes with extremely low noise and deterministic amplification," *Nat. Photon.*, vol. 15, pp. 468–474, 2021.

Joe C. Campbell (Fellow, IEEE) received the B.S. degree in physics from the University of Texas at Austin, Austin, TX, USA, in 1969, and the M.S. and Ph.D. degrees in physics from the University of Illinois at Urbana-Champaign, Champaign, IL, USA, in 1971 and 1973, respectively. From 1974 to 1976, he was employed by Texas Instruments, Dallas, TX, USA, where he worked on integrated optics. In 1976, he joined the staff of AT&T Bell Laboratories, Holmdel, NJ, USA. With the Crawford Hill Laboratory, Holmdel, TX, USA, he worked on a variety of optoelectronic devices including semiconductor lasers, optical modulators, waveguide switches, photonic integrated circuits, and photodetectors with emphasis on high-speed avalanche photodiodes for high-bit-rate lightwave systems. In January of 1989, he joined the Faculty of the University of Texas at Austin as a Professor of electrical and computer engineering and Cockrell Family Regents Chair of engineering. In January of 2006, he became a Member of the Faculty, University of Virginia, Charlottesville, VA, USA, as the Lucian Carr, III Chair of Electrical Engineering and Applied Science. He has coauthored ten book chapters, 490 articles for refereed technical journals, and more than 450 conference presentations. His research focused on the optoelectronic components that are used to generate, modulate, and detect the optical signals. He is actively involved in single-photon-counting avalanche photodiodes, Si-based optoelectronics, low-noise avalanche photodiodes, and high-speed, high-power, high-linearity photodiodes. He is a Member of the National Academy of Engineering.